Journal of Alloys and Compounds 495 (2010) 200–204

Contents lists available at ScienceDirect

Journal of Alloys and Compounds

journal homepage: www.elsevier.com/locate/jallcom

Highly stable Fe–Ni alloy nanoparticles encapsulated in carbon nanotubes: Synthesis, structure and magnetic properties

M.H. Xu[a,b], W. Zhong[a,*], X.S. Qi[a], C.T. Au[c], Y. Deng[a], Y.W. Du[a]

[a] Nanjing National Laboratory of Microstructures and Department of Physics, Nanjing University, Nanjing 210093, China
[b] Department of Applied Physics, Nanjing University of Technology, Nanjing 210009, China
[c] Chemistry Department, Hong Kong Baptist University, Hong Kong, PR China

ARTICLE INFO

Article history:
Received 12 September 2009
Received in revised form 22 January 2010
Accepted 22 January 2010
Available online 2 February 2010

PACS:
61.66.Dk
68.37.Hk
75.75.+a

Keywords:
Composite
FeNi alloy
Magnetization

ABSTRACT

Highly stable Fe–Ni alloy nanoparticles encapsulated in carbon nanotubes have been synthesized by *in situ* catalytic decomposition of benzene over Fe–Ni alloy nanoparticles generated through procedures of sol–gel fabrication and hydrogen reduction. The phases of graphite and γ-FeNi solid solution (face centered cubic) were identified by X-ray diffraction. The results of FE-SEM and HRTEM characterization revealed that Fe–Ni nanoparticles encapsulated in carbon nanotubes are generated in large quantity. The composites are highly stable in air and show soft magnetic property, with saturation magnetization affected by the composition of Fe–Ni alloy and the temperature of benzene decomposition.

1. Introduction

From the viewpoints of fundamental as well as applied research, the studies of the structure and properties of Fe-based alloys are important. Iron is among the most abundant elements on Earth, and is probably the major alloy component for the modern industry. The Fe and Ni elements can form a solid solution in all concentrations but the interesting alloys (such as permalloy A, B and INVAR) are those of fcc phase starting at a Ni composition of 28 mol%. The major feature of the Fe–Ni alloy system is a nearly vanishing thermal expansion coefficient of the $Fe_{0.65}Ni_{0.35}$ alloy as discovered by Guillaume and Hebd in 1897, known as the Invar effect [1]. With other special properties of Fe–Ni alloys such as shape memory, soft magnetization, and martensitic bcc–fcc phase transition with increasing concentration of Ni, Fe–Ni alloys are used in aircraft engines, laser systems, bimetallic thermostats, steam turbines in power generation plants and in medical, nuclear, chemical and petrochemical industries [2,3].

Nanoparticles of transition metals have properties that are significantly different from those of the corresponding bulk materials. However, the investigations and applications of these materials are restricted because they have a great affinity to oxygen and may ignite spontaneously in air even at room temperature (RT). The studies of the nanoparticles must therefore be performed *in situ* in ultrahigh vacuum or in reducing and inert atmospheres [4]. On the other hand, Fe and its alloys (such as the Fe–Ni alloys) are soft magnetic materials that show high specific saturation magnetization, low coercivity and high Curie temperature. Nonetheless, due to their metallic characteristics and the generation of eddy currents, their applications at high frequencies are severely limited [5].

The encapsulation of metallic particles inside a carbon shell is of considerable interest because the encapsulated species can be immunized against environmental degradation [6]. The approach offers an opportunity to investigate the dimensionally confined systems [7], consequently opening a broad range of promising applications, especially in information technologies and biomedicines [8,9]. Compared to the polymer and silica shells that are widely studied, shells made of carbon exhibit much higher stability in various chemical and physical environments such as in acid or base media, and at high temperatures and pressures. It is possible to introduce metals inside the hollow part of carbon nanotubes (CNTs). The introduction of 'foreign' materials may significantly alter the conducting, electronic or mechanical behavior of CNTs. The fabricated composite materials are typically used in technologies such as magnetic data storage devices [10–12], fuel

* Corresponding author. Fax: +86 25 83595535.
E-mail address: wzhong@nju.edu.cn (W. Zhong).

0925-8388/$ – see front matter © 2010 Elsevier B.V. All rights reserved.
doi:10.1016/j.jallcom.2010.01.121

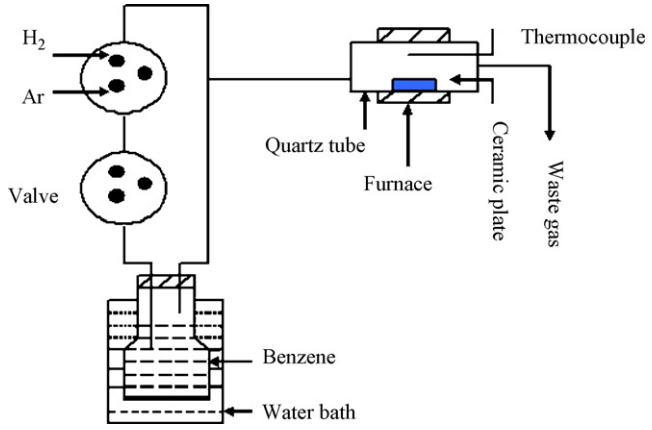

Fig. 1. Experimental setup.

cells [13,14], electromagnetic wave absorption [15,16], sensors for magnetic force microscopy [17] and human tumor therapy [18,19].

In the past decade, various techniques for encapsulating metals, alloys, metal oxides and chlorides in multi-walled or single-walled CNTs have been developed [20–22]. Herein, we report the encapsulation of Fe–Ni nanoparticles in CNTs by *in situ* catalytic decomposition of benzene in an Ar atmosphere at a temperature within the 430–600 °C range over freshly prepared FeNi alloy nanoparticles. The structure and magnetic properties of the composites (i.e. Fe–Ni alloy nanoparticles encapsulated in CNTs) were studied in detail.

2. Experimental

Two steps were used to synthesize the composites: (i) the preparation of Fe–Ni alloy nanoparticles and (ii) the simultaneous synthesis of CNTs and encapsulation of Fe–Ni nanoparticles. The experimental setup is shown in Fig. 1.

All the reagents were of analytical grade and used as received. To prepare the Fe–Ni nanoparticles, 0.03 mol $FeCl_2{\cdot}4H_2O$, quantitative amount of $NiCl_2{\cdot}6H_2O$ (Fe:Ni atomic ratios = 1:3, 2:2, and 3:1) and 0.045 mol citric acid monohydrate were dissolved in 250 mL absolute ethanol (while stirring at 60 °C for 6 h). The as-obtained mixture was kept at 80 °C for several hours, and then heated to 150 °C for the generation of a xerogel. Subsequently, the xerogel was heated in air at 500 °C for 4 h for the generation of the iron-nickel oxide (i.e. Fe_2O_3/NiO powder). To obtain the composites of FeNi alloy and CNTs in large quantity, a quartz tube reactor (6 cm in inner diameter and 75 cm in length), equipped with temperature and gas-flow controls was utilized. The iron-nickel oxide powder (30 mg, spread on a ceramic plate) was placed inside the reactor, and reduced to the iron-nickel nanoparticles with H_2 at 500 °C for 4 h. The FeNi alloys obtained with Fe:Ni atomic ratios equal to 1:3, 2:2, and 3:1 are denoted hereafter as FeNi13, FeNi22, and FeNi31, respectively. Then benzene (kept in a three-necked flask maintained at 70 °C in a water bath) was carried into the reactor in an argon flow. The decomposition of benzene was conducted *in situ* over the freshly prepared FeNi alloy nanoparticles at 500 °C for 6 h, and after cooling to RT, the as-prepared composites (black in color) were collected (denoted hereinafter as FeNi13@C, FeNi22@C, and FeNi31@C, respectively). The samples were examined at RT on an X-ray powder diffractometer (XRD) for phase identification using CuK_α radiation (Model D/Max-RA, Rigaku, Japan). Samples morphology was examined with a high resolution transmission electron microscope (HRTEM, model JEOL-2010, Japan) operated at an accelerating voltage of 200 kV, and a field-emission scanning electron microscope (FE-SEM model 1530VP, LEO, Germany; equipped with a JEOL JFC-1600 auto fine-coater) operated at an accelerating voltage of 5 kV. The resistivity (ρ) of the samples was measured at RT by standard direct-current four-probe technique using a Model-6000 physical property measurement system (PPMS). The magnetic properties of samples were measured at 300 K over a Quantum Design MPMS SQUID magnetometer (Quantum Design MPMS-XL, U.S.A.). The square samples (long 4.5 mm, width 3.5 mm, thickness 0.5 mm) were fabricated for measuring static state hysteresis loop. The complex permeability μ of a composite sample which contained 30 wt% of FeNi13@C (pressed into a ring with outer diameter of 7 mm and inner diameter of 3 mm with paraffin being binder matrix), was measured using an Agilent PNA E8363B (USA) network analyzer in the frequency range of 2 to 18 GHz. Thermoanalysis was carried out on a thermal analysis system (PerkinElmer TGA7 series) with ca. 5.0 mg of sample heated in air at a rate of 10 °C min^{-1}.

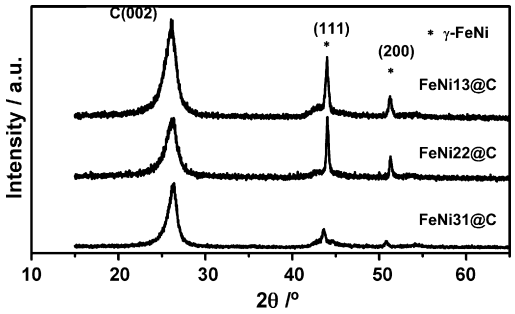

Fig. 2. XRD patterns of composites obtained at 500 °C.

3. Results and discussion

3.1. Structure and morphology of as-prepared composites

In this study, 30 mg of the iron-nickel oxide powder (containing ca. 22.99, 22.26 and 21.62 mg of FeNi13, FeNi22, and FeNi31, respectively) was used and about 0.517, 0.379, and 0.592 g of as-prepared composites of FeNi13@C, FeNi22@C, and FeNi31@C were obtained at 500 °C in each run, respectively.

The XRD patterns of the composites obtained over FeNi13, FeNi22, and FeNi31 at 500 °C are shown in Fig. 2. A reflection at 26.22° can be attributed to (0 0 2) plane of hexagonal graphite (JCPDS Card File No. 41-1487, lattice parameters a = 2.470 Å and c = 6.756 Å), denoting the formation of graphitic species. Reflections at 43.92° and 51.22° can be indexed, respectively, to (1 1 1) and (2 0 0) planes of fcc γ-FeNi alloy (JCPDS Card File No. 47-1417, lattice parameter a = 3.597 Å). There is no XRD signal assignable to pure Fe and Ni metals. These results suggest that the as-prepared composites are composed of graphite and Fe–Ni alloy nanoparticles. Using the Scherrer formula with deal consideration to the FWHM (full width at half maximum) of the (1 1 1) peak of Fe–Ni alloy, the average grain size of Fe–Ni alloy is estimated to be 18.7, 27.9, and 13.9 nm for FeNi13@C, FeNi22@C, and FeNi31@C, respectively.

Representative FE-SEM images of as-prepared composites obtained at 500 °C are shown in Fig. 3. It can be observed that composites of one-dimensional nanostructure with irregular morphology are formed. There is no direct relationship between the

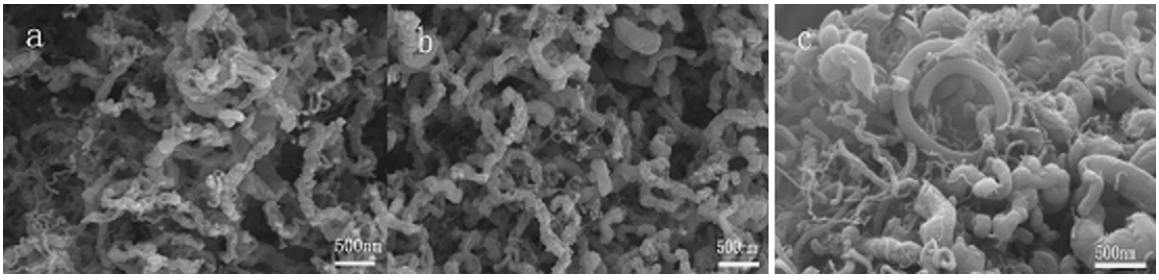

Fig. 3. FE-SEM images of as-prepared composites: (a) FeNi13@C, (b) FeNi22@C, and (c) FeNi31@C.

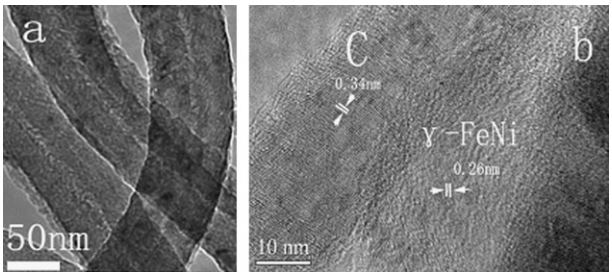

Fig. 4. HRTEM micrograph of composites obtained at 500 °C: (a) FeNi13@C and (b) FeNi31@C.

Table 1
Magnetic parameters of composites prepared at 500 °C.

Samples	H_C/Oe	M_S/emu g^{-1}	M_S/emu g^{-1} of FeNi alloy	Initial permeability
FeNi13@C	47	4.48	100.75	1.0674
FeNi22@C	68	8.32	141.66	1.1128
FeNi31@C	207	3.32	90.91	1.0746

morphology of the composites and the composition of the Fe–Ni alloy nanoparticles. Crystallite size of FeNi13@C and FeNi22@C is in the 100–150 nm range, smaller than that of FeNi31@C. The product of benzene decomposition over the Fe–Ni alloys is different from that over Ni metal nanoparticles. In the latter case, nanorods composed of carbon nanoflakes were generated [23].

Fig. 4 shows HRTEM micrographs of composites obtained at 500 °C. The average wall thickness of CNTs is ca. 40 nm. The inner diameter of CNTs ranges from 8 to 12 nm. As shown in Fig. 4b, the lattice fringes of graphite and FeNi alloy can be clearly seen. The average value of spacing of graphitic sheets is about 0.34 nm, consistent with XRD results. Lattice edges of FeNi alloy are about 0.26 nm, in good agreement with the interlayer separation of the (1 1 1) crystal plane of γ-FeNi.

3.2. Magnetic properties and stability of as-prepared composites

The magnetization of the composites versus field were measured at RT. Fig. 5 shows the magnetization–coercivity (*M–H*) curves of the composites prepared at 500 °C, and the related results are listed in Table 1. The coercivity of FeNi13@C, FeNi22@C, and FeNi31@C is 47, 68 and 207 Oe, respectively, indicating that the coercivity of the composites increases with the rise of Fe concentration in the Fe–Ni alloys. The results coincide well with the

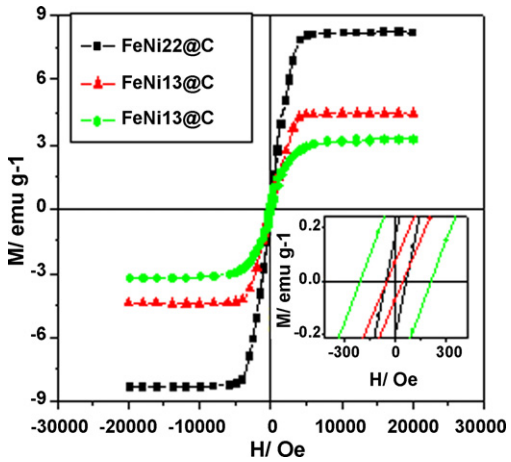

Fig. 5. Typical magnetization curves of composites prepared at 500 °C. The inset shows enlarged part of the curves close to the origin.

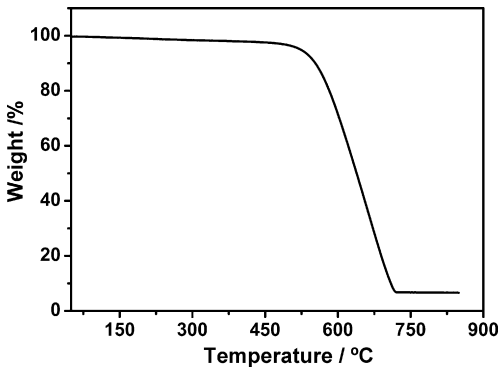

Fig. 6. TG curve of composite FeNi22@C.

results of Wu et al. [24]. According to the theoretical prediction using the random-anisotropy model (RAM) [25], the coercive field is inversely proportional to the six power of the grain size *D* when the ferromagnetic exchange length exceeds the grain size. In other words, the smaller the grain size, the larger the coercivity. The average grain size of FeNi31 is the least (ca. 13.9 nm) among the three FeNi alloys and the coercivity of FeNi31@C is the largest. Nevertheless, to a large extent coercivity is an extrinsic property determined by the microstructure of sample; other factors such as morphology of sample and processing procedures may influence the value of coercivity.

Table 1 shows that the saturation magnetization M_S (emu g^{-1} of FeNi alloy) reaches its maximum value (141.66 emu g^{-1}) over FeNi22@C. The M_S (emu g^{-1} of FeNi alloy) is enhanced in the order of FeNi31 < FeNi13 < FeNi22. This result is consistent with the trend of the saturation induction of FeNi alloys at RT [26,27]. There are two specific concentrations of Ni in Fe–Ni alloys worth mentioning, namely, the Ni-rich permalloy alloy (35–80 wt% Ni) and the Fe-rich invar alloys (65 wt% Fe). Bozorth [27] reported that the saturation induction exhibits a dramatic change with Ni concentration. It exhibits the maximum value at about 50 wt% Ni and then decreases in the Ni-rich region at RT. The saturation induction decreases with increasing Ni concentration in the Fe-rich region. The drop in saturation induction near 30 wt% Ni at RT corresponds to the steep decrease in Curie temperature in this region [26,27]. FeNi13 (Ni concentration 76 wt%) and FeNi22 (Ni concentration 51 wt%) of our samples belong to the Ni-rich alloy. The magnetization of FeNi22 is larger than that of FeNi13. The FeNi31 (26 wt% Ni) sample belongs to the Fe-rich alloy, and M_S is lowered to 90.91 (emu g^{-1} of FeNi alloy). This experimental phenomenon may be explained by the energy-band model and the Slater–Pauling curve [28,29]. The energy-band model [29] indicates that in a ferromagnetic alloy, an increase of electrons number in the d band can enhance or decrease electron distribution of energy-band, and hence change the magnetic moment of the alloy. The Slater–Pauling curve [28] indicates that the average magnetic moment of alloy is a function of the amount of outer electrons. In the cases of this study, the addition of Ni in the Fe-rich region enhances electron distribution and hence a decline of magnetic moment, whereas the addition of Fe in the Ni-rich region would result in an opposite effect. When the Ni content is around 50 wt%, the amount of positive-spin electrons reaches its maximum, and magnetic moments start to decline. In addition there is an interaction between the ferromagnetism of FeNi alloy and diamagnetism of carbon [30], making the magnetic properties of FeNi–CNTs composites complicated.

The thermogravimetric curve of composite FeNi22@C shows a weight loss in the 500–720 °C range and a residue of 6.99 wt% (Fig. 6). The loss is ascribed to carbon oxidation and the residue can be ascribed to FeNi oxide.

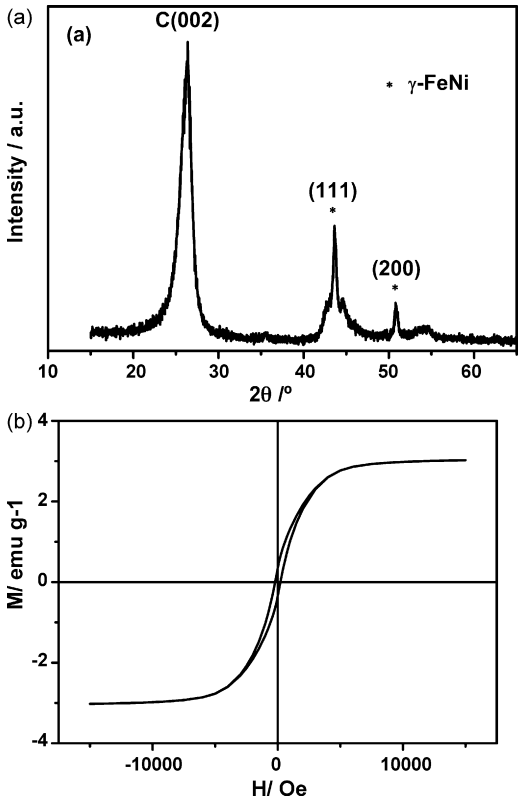

Fig. 7. (a) XRD pattern and (b) *M–H* curve of composite FeNi31@C that have been exposed to environment for over 300 days.

The XRD pattern and *M–H* curve of FeNi31@C composite that has been exposed to environment over 300 days are shown in Fig. 7. A comparison of the data of Figs. 2, 5 and 7 indicates that the XRD features and magnetic properties are not significantly altered. The XRD patterns look very similar, and the M_S (ca. 3.06 emu g^{-1} in Fig. 7) and H_C (ca. 213 Oe in Fig. 7) of the samples are also quite close (M_S = 3.32 emu g^{-1}, H_C = 207 Oe in Fig. 5). In the FeNi–CNT composites, the encapsulated metal alloy is effective protected by CNTs against oxidation, resulting in high magnetization and high stability of the FeNi–CNT materials.

The resistivity (ρ) of FeNi31@C is about 1.5 Ω cm at RT, remarkably larger than that of pure Fe–Ni alloy. Eddy current loss is inversely proportional to resistivity. The frequency dependence of the complex permeability of FeNi31@C composite is shown in Fig. 8. One can see that the real part μ' and imaginary part μ'' fluctuate with frequency. The imaginary part μ'' is almost zero, reaching a maximum of 0.21 at 12 GHz. With the decline of μ'', there is a reduction in magnetic loss.

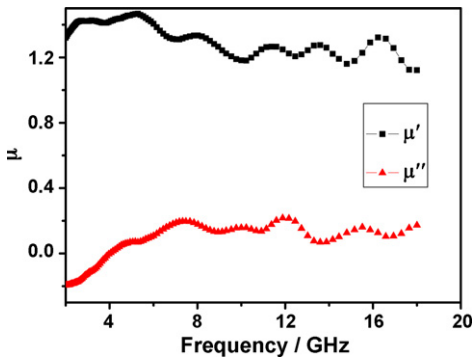

Fig. 8. The complex permeability of FeNi31@C composite.

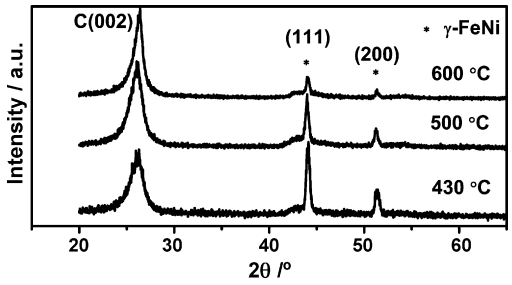

Fig. 9. XRD patterns of composite FeNi13@C prepared at different temperatures.

Table 2
Magnetic parameters of FeNi13@C composite prepared at different temperatures.

Reaction temperature/°C	H_C/Oe	M_S/emu g^{-1}	M_S/emu g^{-1} of FeNi alloy
430	133	7.14	106.87
500	47	4.48	100.75
600	190	2.94	66.24

3.3. Effect of benzene decomposition temperatures

In this study, the effects of benzene decomposition temperature on the yield and magnetic properties of the composites were also investigated. We found that the decomposition temperature has distinct influence on the yield as well as on the magnetic properties of the composites. The benzene decomposition reaction was carried out at 430, 500, and 600 °C for 6 h over the freshly prepared FeNi13 nanoparticles (ca. 22.99 mg), and about 0.344, 0.517, and 0.518 g of FeNi13@C was collected, respectively. Fig. 9 shows the XRD pattern of FeNi13@C obtained at 430, 500 and 600 °C. Again, the diffraction peaks can be indexed to phases of graphite and γ-FeNi alloy. It is apparent that the yield of composite increases with the increase of the reaction temperature.

Fig. 10 shows the magnetic properties of the FeNi13@C samples generated at 430, 500 and 600 °C, and the magnetic parameters are listed in Table 2. The M_S (emu g^{-1} of FeNi alloy) is 106.87, 100.75 and 66.24, respectively. The M_S (emu g^{-1} of FeNi alloy) decreases with increasing decomposition temperatures. In contrast to the disordered state, atomic ordering occurs in the vicinity of the $FeNi_3$ composition, causing an increase in the value of saturation induction. The property of FeNi alloy with composition near that of $FeNi_3$ is susceptible to the change of temperature [26,27]. According to the phase graph of FeNi alloy, the long-range order structure of $FeNi_3$ appears at about 500 °C. We deduce that increasing temperature causes a destruction of the atomic ordering of $FeNi_3$. This can be well described by the theory developed by Sidorov and Doroshenko

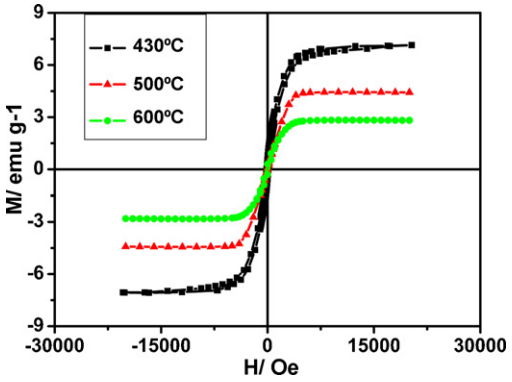

Fig. 10. Typical magnetization curves of composite FeNi13@C prepared at different temperatures.

[31] in which the Fe–Fe interaction is considered antiferromagnetic and the Ni–Ni and Fe–Ni interaction ferromagnetic. The saturation magnetization at RT is dependent on the number of closest neighboring Ni atoms surrounded by Fe atoms. It is reported that some Fe atoms (Fe′, Fe atoms that are surrounded by five or less than five nearby Ni atoms) in the γ-FeNi alloy have localized moments, giving rise to a high magnetic moment of 2.8 μ_B [24,32]. However, localized moments on Fe atoms vanish and paramagnetic Fe atoms (Fe″, Fe atoms that are surrounded by 5–12 nearby nickel atoms) are produced. The detailed magnetic properties of these materials need to be further investigated.

Table 2 shows that the coercivity of the FeNi13@C samples generated at 430, 500 and 600 °C are 133, 47 and 190 Oe, respectively. The coercivity is at its minimum over the FeNi13@C composite generated at 500 °C, whereas at its maximum over the FeNi13@C composite generated at 600 °C. The cause of such a phenomenon is perhaps hard to identify because coercivity is known to be sensitive to many structural parameters such as internal stress, orientation, defects, and shape [33]. Nevertheless, it is clear that by controlling the composition of the alloy through adjusting the Fe to Ni atomic ratio and by controlling the temperature of benzene decomposition, the magnetic property of the FeNi–CNT composites can be optimized for applications in different fields.

4. Conclusions

By means of sol–gel and hydrogen reduction followed by benzene decomposition, we prepared composites of FeNi alloy and CNTs. It was found that the composites are highly stable when exposed to environment, probably due to the encapsulation of the FeNi alloy nanoparticles inside a protective wall of graphitic carbon. The magnetic properties of the FeNi–CNT composites can be optimized by adjusting the composition of the alloy or by controlling the temperature for benzene decomposition. We envisage that the materials have wide applications in fields such as microwave absorption, magnetic storage and human tumor therapy.

Acknowledgements

This work was supported by the National Natural Science Foundation of China (Grant No. 10674059), the National High Technology Research and Development Program of China (Grant No. 2007AA021805), and the National Key Project for Basic Research (Grant Nos. 2005CB623605 and 2010CB923402), People's Republic of China.

References

[1] C.E. Guillaume, C.R. Hebd, Seances Acad. Sci. 125 (1897) 235.
[2] E. Gonzalez, P. Jasen, G. Gonzalez, L. Moro, A. Juan, Phys. Status Solidi B 246 (2009) 1275–1285.
[3] Kh. Gheisari, S. Javadpour, J.T. Oh, M. Ghaffari, J. Alloys Compd. 472 (2009) 416–420.
[4] F.B. Dker, S.M. Rup, S. Linderoth, Phys. Rev. Lett. 72 (1994) 282–285.
[5] M. Plaza, L. Perez, M.C. Sanchez, J. Magn. Magn. Mater. 309 (2007) 207–211.
[6] H.P. Li, N.Q. Zhao, C.N. He, C.S. Shi, X.W. Du, J.J. Li, J. Alloys Compd. 458 (2008) 130–133.
[7] V.P. Dravid, J.J. Host, M.H. Teng, B. Elliott, J. Hwang, D.L. Johnson, T.O. Mason, J.R. Weertman, Nature 374 (1995) 602–1602.
[8] M.E. McHenry, S.A. Majetich, J.O. Artman, M. DeGraef, S.W. Staley, Phys. Rev. B 49 (1994) 11358–11363.
[9] S. Subramoney, Adv. Mater. 10 (1998) 1157–1171.
[10] H. Terrones, F. López-Urías, E. Muñoz-Sandoval, J.A. Rodríguez-Manzo, A. Zamudio, A.L. Elías, M. Terrones, Solid State Sci. 8 (2006) 303–320.
[11] Z.J. Liu, Z.D. Xu, Z.Y. Yuan, W.X. Chen, W.Z. Zhou, L.M. Peng, Mater. Lett. 57 (2003) 1339–1344.
[12] H.Q. Wu, D.M. Xu, Q. Wang, Q.Y. Wang, G.Q. Su, X.W. Wei, J. Alloys Compd. 463 (2008) 78–83.
[13] E.S. Steigerwalt, G.A. Deluga, C.M. Lukehart, J. Phys. Chem. B 106 (2002) 760–766.
[14] G.L. Che, B.B. Lakshmi, C.R. Martin, E.R. Fisher, Langmuir 15 (1999) 750–758.
[15] H.Y. Wu, Y. Zhao, Q.Z. Jiao, J. Alloys Compd. 487 (2009) 591–594.
[16] R.C. Che, L.M. Peng, X.F. Duan, Q. Chen, X.L. Liang, Adv. Mater. 16 (2004) 401–405.
[17] A. Winkler, T. Muhl, S. Menzel, R. Kozhuharova-Koseva, S. Hampel, A. Leonhardt, B. Büchner, J. Appl. Phys. 99 (2006) 104905-1–104905-5.
[18] I. Mönch, A. Meye, A. Leonhardt, K. Krämer, R. Kozhuharova, T. Gemming, M.P. Wirth, B. Büchner, J. Magn. Magn. Mater. 290 (2005) 276–278.
[19] G. Korneva, H.H. Ye, Y. Gogotsi, D. Halverson, G. Friedman, J.C. Bradley, K.G. Kornev, Nano Lett. 5 (2005) 879–884.
[20] N. Grobert, M. Mayne, M. Terrones, J. Sloan, R.E. Dunin-Borkwski, R. Kamalakaran, T. Seeger, H. Terrones, N. Rühle, D.M.R. Walton, H.W. Kroto, J.L. Hutchison, Chem. Commun. (2001) 471–472.
[21] M. Terrones, N. Grobert, W.K. Hsu, Y.Q. Zhu, W.B. Hu, H. Terrones, J.P. Hare, H.W. Kroto, D.R.M. Walton, MRS Bull. 24 (1999) 43–49.
[22] J. Sloan, D.M. Wright, H.G. Woo, S. Brown, A.P.E. York, K.S. Coleman, J.L. Hutchison, M.L.H. Green, Chem. Commun. (1999) 699–700.
[23] X.S. Qi, M.H. Xu, W. Zhong, X.J. Ye, Y. Deng, C.T. Au, C.Q. Jin, Y.W. Du, J. Phys. Chem. C 113 (2009) 2267–2272.
[24] H.Q. Wu, Y.J. Cao, P.S. Yuan, H.Y. Xu, X.W. Wei, Chem. Phys. Lett. 406 (2005) 148–153.
[25] J.F. Löffler, H.V. Swygenhoven, W. Wagner, J. Meier, B. Doudin, J.P. Ansermet, Nanostruct. Mater. 9 (1997) 523–526.
[26] E.P. Wohlfarth, Ferromagnetic Materials, North-Holland Publishing Company, New York, 1980.
[27] R.M. Bozorth, Ferromagnetism, D.Van Nostrand Co., New York, 1951.
[28] G.F. Koster, J.C. Slater, Phys. Rev. 96 (1954) 1208–1223.
[29] J. Kanamori, K. Terakura, K. Yamada, Prog. Theor. Phys. 41 (1969) 1426.
[30] K. Lafdi, A. Chin, N. Ali, J.F. Despres, J. Appl. Phys. 79 (1996) 6007–6009.
[31] S.K. Sidorov, A.V. Doroshenko, Phys. Status Solidi 16 (1966) 737.
[32] X.G. Diao, A.Y. Takeuchi, F. Garcia, R.B. Scorzelli, J. Appl. Phys. 85 (1999) 4485–4487.
[33] T. Hayashi, S. Hirono, M. Tomita, S. Umemura, Nature 381 (1996) 772–774.